Bioinspired, microstructured silk fibroin adhesives for flexible skin sensors

Liu, Xijian; Liu, Jun; Wang, Jilei; Wang, Ting; Jiang, Ying; Hu, Junqing; Liu, Zhuangjian; Chen, Xiaodong; Yu, Jing

2020

Liu, X., Liu, J., Wang, J., Wang, T., Jiang, Y., Hu, J., . . . Yu, J. (2020). Bioinspired, microstructured silk fibroin adhesives for flexible skin sensors. ACS Applied Materials & Interfaces, 12(5), 5601-5609. doi:10.1021/acsami.9b21197

https://hdl.handle.net/10356/138082

https://doi.org/10.1021/acsami.9b21197

Bio-inspired, Micro-structured Silk Fibroin Adhesives for Flexible Skin Sensors

Xijian Liu,[1,2] Jun Liu,[3] Jilei Wang, [2] Ting Wang,[2] Ying Jiang,[2] Junqing Hu,[4] Zhuangjian Liu[*],[3] Xiaodong Chen,[* 2] Jing Yu[*2]

[1]College of Chemistry and Chemical Engineering, Shanghai University of Engineering Science, Shanghai 201620, P. R. China.

[2]School of Materials Science and Engineering, Nanyang Technological University, 639798, Singapore.

E-mail: chenxd@ntu.edu.sg; yujing@ntu.edu.sg

[3]Institute of High Performance Computing, Agency for Science Technology and Research, 1 Fusionopolis Way, 138632, Singapore.

Email: liuzj@ihpc.a-star.edu.sg

[4]College of Health Science and Environmental Engineering, Shenzhen Technology University, Shenzhen, 518118, China.

ABSTRACT: Wearable epidermal sensors are of great importance to the next generation personalized healthcare. The adhesion between the flexible sensor and skin surface is critical for obtaining accurate, reliable and stable signals. Herein we present a facile approach to fabricate a micro-structured, natural silk fibroin protein based adhesive for achieving highly conformal, comfortable, adjustable, and biocompatible adhesion on the skin surface. The micro-structured fibroin adhesive (MSFA) exhibits reliable and stable bonding force on skin surfaces, even under humid or wet conditions, and can be easily peeled off from the skin without causing significant pain. Such MSFA can greatly improve the sensitivity and reusability of epidermal strain sensors due to its

conformal and tunable adhesion on skin surfaces. The MFSA has a great potential to be applied as functional adhesives for various epidermal electronic sensors in the era of personalized healthcare.

Keywords

Micro-structured adhesives, silk fibroin, high sensitivity, reusable, flexible epidermal sensors

1. INTRODUCTION

Wearable electronic devices can be used as artificial tissue,[1-3] and represent powerful tools towards the long-term health-monitoring due to non-invasive measurement, light weight and high comfort,[4-7] which can monitor heart rate,[8-9] respiration rate,[10] electrocardiograms,[11-13] electroencephalogram,[14] electromyography,[15-17] blood oxygenation,[18] skin temperature,[19-20] body motion[21-22] and blood pressure,[8, 23] etc. To obtain accurate human physical information through skin surface, the adhesion between the skin surface and devices is pivotal. However, it is still a great challenge for the epidermal electronic devices to achieve conformal attachment to the rough, soft and textured surface of skin.[24-27] This challenge is further amplified in hot and humid environments or during exercise, in which the sweat and motion of human body may cause bonding failure (detachment) of many artificial pressure sensitive's adhesives. [28-31]

Another important aspect for epidermal electronic devices is to achieve a suitable range bonding strength of adhesion between pressure sensitive adhesives (e.g. medical tape and plastic bandages) and the surface of skin, which can lead to uncomfortable feelings such as sharp pain during the removal of the devices.[32] People (new-borns, older adults, and medications) with fragile or delicate skin may even experience skin injury during the removal of medical adhesives due to strong adhesion.[11, 33] The next generation moisture-resistant pressure sensitive adhesives with tuneable adhesion is therefore critical for the wide application of epidermal electronic devices.

Nature provides excellent examples for achieving reliable and comfortable adhesion to complex surfaces for epidermal electronic devices.[29-30, 34-36] The hierarchical structure of the gecko foot has inspired numerous studies on developing gecko-inspired skin adhesives.[37-40] The conformal contact between the micro-pillars with skin can also improve the efficiency in conduct mechanical deformations from rough surfaces to the device. However, such devices still needed to use medical tapes and the performance of such structured adhesives on the skin surface under wet or sweating conditions has not been fully investigated. [41-42]

Silk fibroin is a highly biocompatible and biodegradable natural protein that has been widely

employed as polymer based substrates, dielectrics of transistors and water-soluble sacrificial layers.[43-47] Recently, calcium-modified silk fibroin was demonstrated as a biocompatible adhesive for epidermal electronics, and the adhesion of fibroin could be well maintained in environment of the high humidity.[48-49] Thus, it is highly desirable to use silk fibroin as an adhesive on the epi-electronic devices for conformal and comfortable bonding with human skin.

Herein, we present a fabrication and design scheme for fibroin adhesives with micro-pillar structures on PDMS substrate, which we denote Micro-Structured Fibroin Adhesive (MSFA) (Figure 1a). The MSFA shows strong and tunable adhesion on human skin even under humid conditions, and can be readily integrated into epidermal electronic devices. A flexible strain sensor with a MSFA layer was fabricated, which showed a conformal, firm and comfortable adhesion on the surface of human skin (Figure 1b).

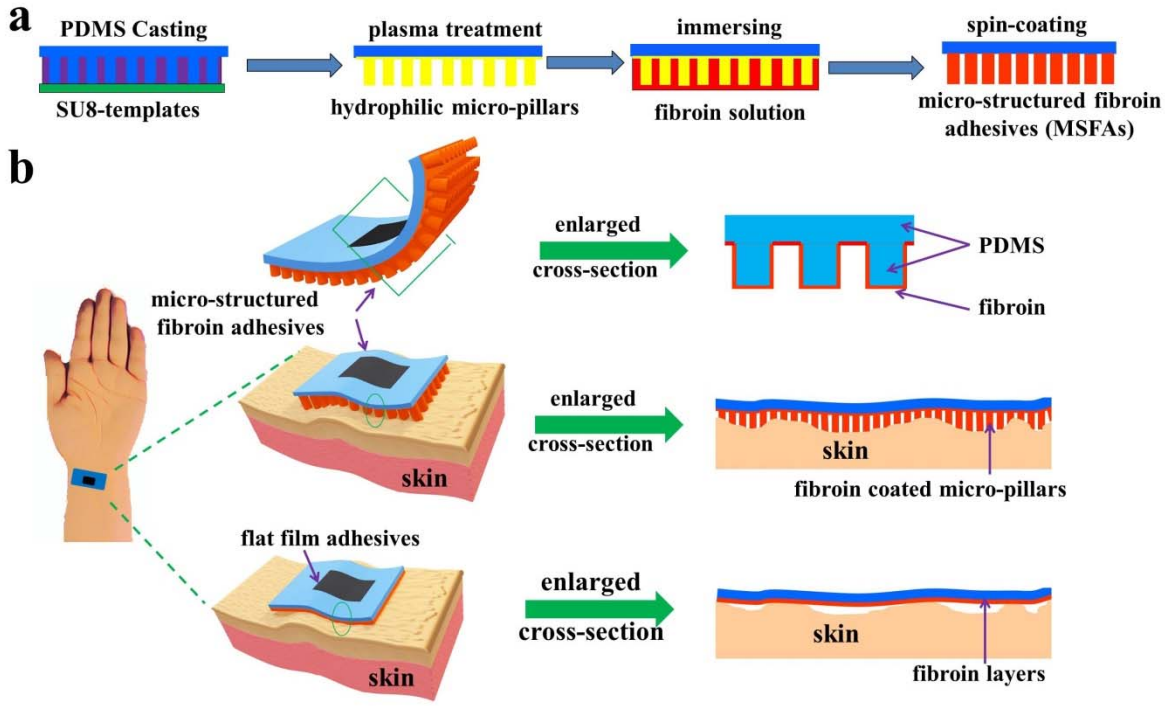

Figure 1 (a) Fabrication process of micro-structured fibroin adhesive (MSFA): preparation of the PDMS micro-pillars film, plasma treatment and silk fibroin coating. (b) A schematic of an MSFA on the surface of wrist skin. The MSFA is highly flexible and conformal on the rough skin surface

due to the micro-pillar structure, whereas a flat silk fibroin adhesive layer cannot perfectly attach to the skin.

2. RESULTS AND DISCUSSION

2.1. MSFA fabrication and characterizations

The MSFA is constituted by PDMS micro-pillars coated with fibroin (Figure 1a). Firstly, PDMS micro-pillars were fabricated using a template method. After oxygen plasma treatment, the PDMS micro-pillars were dipped into a silk fibroin solution (weight ratio of silk: formic acid:$CaCl_2$ is 1:4:0.4) followed by spin coating at speed of 700 rpm/min, forming a silk fibroin adhesive layer on top of the PDMS micro-pillars. The effects of the micro-pillar geometry on the adhesion of fibroin were investigated systematically through the measurement of adhesions of various micro-pillar geometrical dimensions. PDMS micro-pillars at different diameters, 20, 40, 60, and 80 μm, were fabricated in regular arrays with a spacing distance of 100 μm between the centers of two pillars (Figure S1). Coating the pillars with fibroin slightly increased their diameter (Figure 2a and Figure S1 and S2). The bonding force between PDMS micro-pillars and a bare spherical glass disk (R=5 cm) was measured using the tensile testing instrument with a Johnson, Kendall, and Roberts (JKR) geometry[50]. (Figure S3a). The measured bonding force, F, was converted to the adhesion energy based on JKR theory, $E=2F/3\pi R$. As expected, the bonding force as a function of load increased with the diameter of the pillars increased, due to the increase of the contact area and mechanical stability of the pillars (Figure S3b, c). The bonding forces of three micro-pillars with different pillar heights, 40, 80, and 120 μm, were measured with a fixed diameter of 80 μm. The adhesion force slightly decreased as we increased the pillar height as PDMS pillars with larger heights were easier to buckle. Microscopic image of the skin surface (artificial PDMS skin replica) revealed that the skin surface is composed of island-like planar areas and the microgrooves have a vertical roughness of around ~70 μm (Figure S4). To achieve a better on-skin adhesion and easy fabrication, the micro-pillars with diameter of 80 μm and height of 80 μm were chosen for further study.

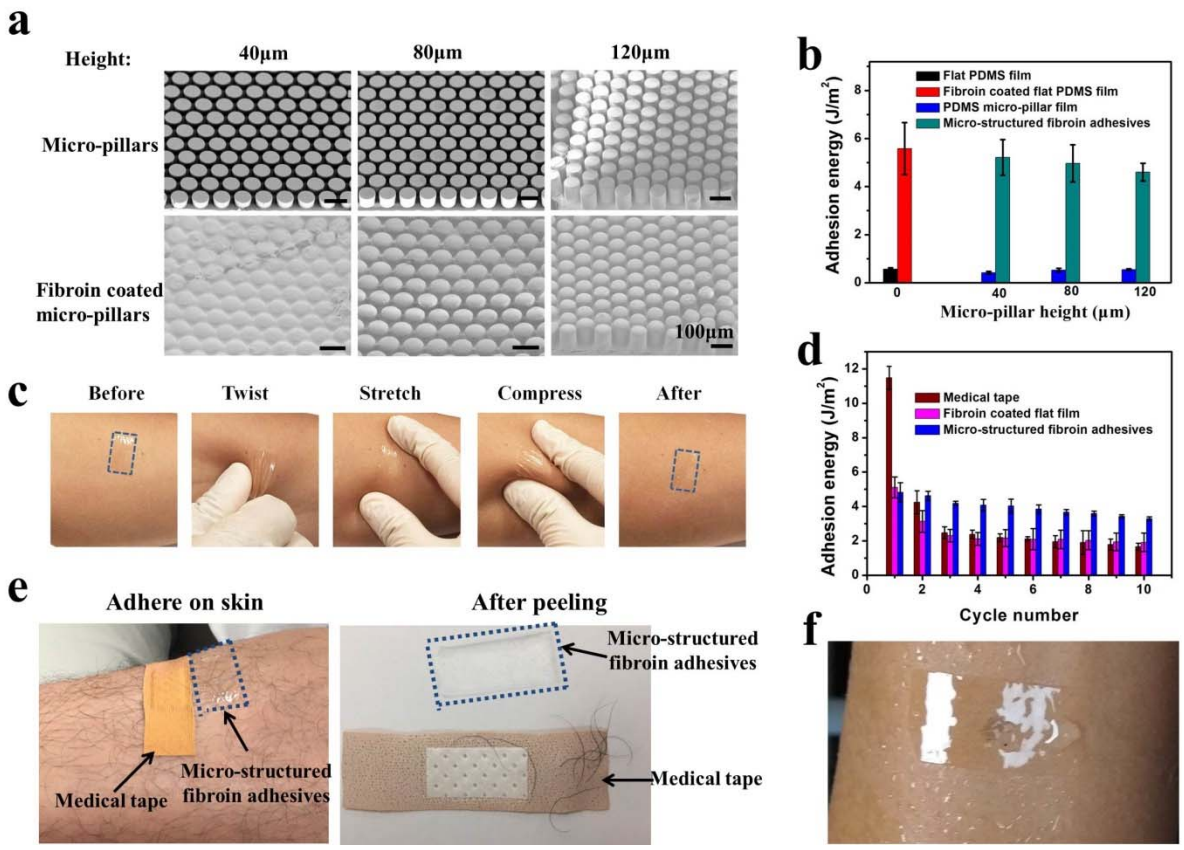

Figure 2 Bio-inspired micro-structured fibroin adhesives. (a) SEM images of bare (top) and fibroin (bottom) coated micro-pillars with a diameter of 80 μm and heights of 40 μm (left), 80 μm (middle),120 μm (right). (Scale bar: 100 μm). (b) Adhesion energies of a flat PDMS film, a fibroin coated flat film, a PDMS micro-pillar film and MSFAs of different pillar heights against a spherical glass surfaces (R = 5 cm). (c) Photos of an MSFA before and after twisting, compression and stretching on human skin (The dotted box indicates the micro-pillars film). (d) The adhesion energy of medical tape, fibroin coated flat and an MSFA in 10 conservative tests. The MSFA can preserve ~70% of its original adhesion strength. (e) Commercial medical tape can lead to hair stripping during its removal process while the MSFA did not strip any hair during the peeling process. (f) The MSFA can firmly adhere to the skin in humidity conditions.

2.2.The adhesion and peeling properties of MSFA

The fibroin coating greatly improves the adhesion between the micro-structured PDMS film and human skin. The MSFA is firmly bonded on the skin surfaces of the forearm and maintained its position without detachment after various deformation such as twisting, stretching, compressing and strenuous movements (Figure 2c and movie S1). Various amino acid residues in the silk fibroin protein can form hydrogen bonds with the skin surface, leading to strong adhesion.[51] Additionally, the good viscoelastic properties of silk fibroin protein in the presence of Ca^{2+} lead to a good contact at the interface and appropriate cohesion.[48] The bonding strength can also be easily tuned by controlling the density and diameter of the micro-pillars. This tunability is useful in many applications, such as medical adhesive tapes for sensitive skins.

To evaluate the durability of the MSFA, we compared the bonding forces of a MSFA and a commercial medical tape in cycling tests. As shown in Figure 2d, the commercial medical tape showed the highest adhesion energy (11.48 J/m^2) in the first cycle. However, its adhesion energy decreased significantly in the following cycles. After loading and unloading repeated 10 times, the adhesion energy of the commercial medical tape was only 1.67 J/m^2, about 15% of the value in the first cycle. The dramatic decreasing of adhesion was mainly due to the cohesion reduced in the adhesive layer. During the cycling test, the residues of adhesives were found on the glass disk, which could be the main reason for the reduced bonding force in the subsequent cycles. A flat fibroin film on a PDMS substrate also displayed a similar monotonic decrease of adhesion energy. In contrast, the MSFA had the lowest adhesion energy to the glass substrate at the initial cycle (4.83 J/m^2); whereas, it showed superior durability during the following cycles. The adhesion energy only decreased by about 30% after 10 cycles. The lower initial adhesion of MSFA was mainly caused by a smaller contact area with the substrate due to the microstructure. The smaller contact area also minimums the possibility of adhesive failure of the fibroin adhesive layer during the separation. Therefore, the stable bonding force is observed during the consecutive tests.

One shortage of the commercial medical adhesives is the unpleasant sharp pain caused during the device or tape removing since there is a strong adhesion between skin surface and substrate. Thanks

to the tunability of the MSFA, such shape pain can be greatly reduced or even fully avoided. The 180° peeling forces were measured for a commercial medical tape, a flat fibroin adhesive film and an MSFA on PET substrates, respectively (Figure S3d). The MSFA showed the lowest peeling force of 61.5 N/m at a peeling speed of 5 mm/min, whereas the medical tape showed a high peeling force of 162.6 N/m. To further demonstrate that the MSFA can reduce the shape pain during the adhesive peeling process, we peeled a medical tape and an MSFA adhered on the skin at a fix peeling angle of 90°. The skin deformed significantly when pulling off the medical tape, resulting in sharp pain (Figure S5). It was also found that some androgenic hairs were peeled off by the medical tape in the tests (Figure 2e). In comparison, there was no obvious deformation of the skin surface when pulling off the MSFA. No androgenic hair was peeled off and no significant pain was reported during the MSFA peeling process (Figure 2e and movie S2). This clearly shows that the micro-pillar structure of the MSFA can decrease the peeling force during the removal of the adhesives, which can greatly reduce the discomfort during the adhesive removal process.

The MSFA can firmly bonding on the skin under higher humidity and sweating conditions (Figure 2f). We adhered a medical tape and an MSFA on the surface of skin of wet forearm (mixture of sweat and water), then performed excise. The medical tape detached from skin during excise, whereas the MSFA is still firmly sticked on the skin surface (Figure S6 and movie S3). The 90° peeling force (with a peeling speed of 0.1 mm/s) of the MSFA on a pre-wetted forearm skin was 18.8±3.7 N/m. Therefore, they could function very well in high humidity environment and large motion activates. Biocompatibility is another very important advantage for this type of adhesives. The skin of bonded area showed no difference from the other part of skin after using the MSFA for more than 8 hours, and no hypersensitivity was observed (Figure S7). The microstructure also provide the MSFA excellent gas permeability due to the space between the micropillars as well as the good gas permeabilities of silk fibroin and PDMS.[28, 52]

2.3. Fabrication of MSFA strain sensors and their Synchronous electro-mechanical characterization

The excellent flexibility and on-skin adhesive properties, as well as the easy peeling of the MSFA make it a high potential candidate as adhesives element for epidermal devices, such as flexible electronic sensors, which often require good conformability and stable adhesion on human skin to provide a mechanical interface between the human skin and the epidermal devices. To demonstrate such possibility, we fabricated a flexible strain sensor with a MSFA layer and a SWCNTs net layer by dropping the SWCNTs solution on the PDMS film (Figure 3a and Figure S8). The length and width of the SWCNT ring in the MSFA sensor were ~ 8 mm and ~ 6 mm, respectively. We denote it the MSFA strain sensor in the following session.

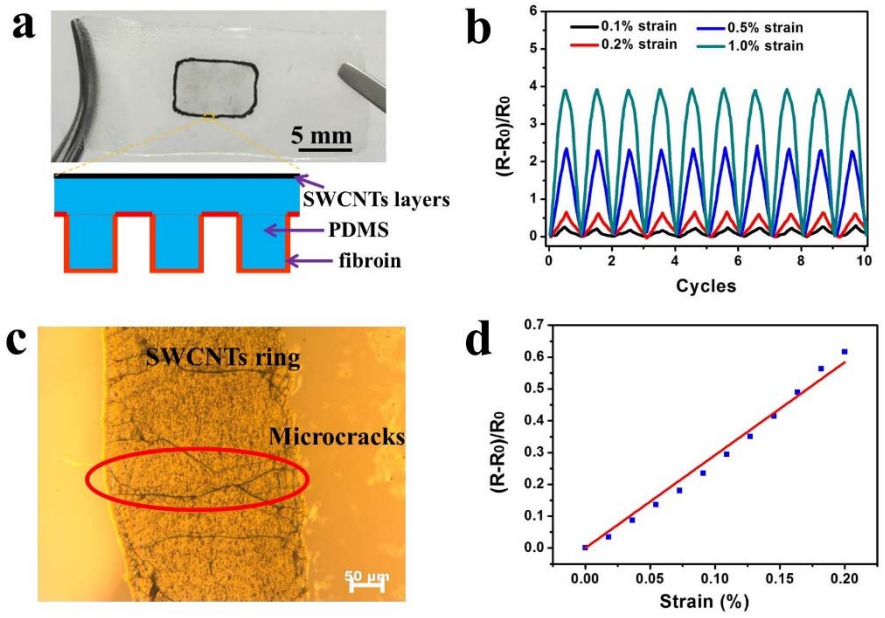

Figure 3 Flexible strain sensor with micro-structured fibroin adhesives. (a) A photo of the flexible strain sensor with the MSFA (upper) and the cross section schematic of the sensor (lower). (b) Normalized resistance change of the MSFA strain sensor with 0.1%, 0.2%, 0.5%, and 1.0% strain. Small strain leads to significant resistance changes. (c) The microscope images of SWCNTS ring after tension, which showed SWCNTs' densely accumulated and many micro-cracks distribute in the SWCNTs ring. (d) Normalized resistance change as a function of the strain from 0 to 0.2% shows good linear relationship.

The MSFA strain sensor is highly flexible and easily attached on human skin. Figure 3b shows the durability behavior of the fabricated sensor under repeated stretching-releasing cycling. The sensor

showed large electrical resistance change as the strain of the sensor increased from 0.1% to 1% with a gauge factor of ~392. The high sensitivity of the MSFA strain sensor could be ascribed to the micro-crack's opening-closing mechanism of the SWCNTs net layer under stretching-releasing cycling (Figure 3c and Figure S9).[24, 53] When increasing the strain from 0% to 0.2%, the normalized electrical resistance change showed a very good linearity with the tensile strain (Figure 3d), which is essential for precise measurement of small strain (such as pulse). The normalized resistances change of the sensor as a function of the strain showed no obvious change before and after 10 times peeling-attaching tests (Figure S9d). The fabricated micro-structured strain sensor also showed good cycling durability with more than 1700 cycling loadings (Figure S9e), which is demonstrated stable ability under large number of cycling.

2.4. Pulse measurement by MSFA strain sensors and their Strain distribution from FEM simulation

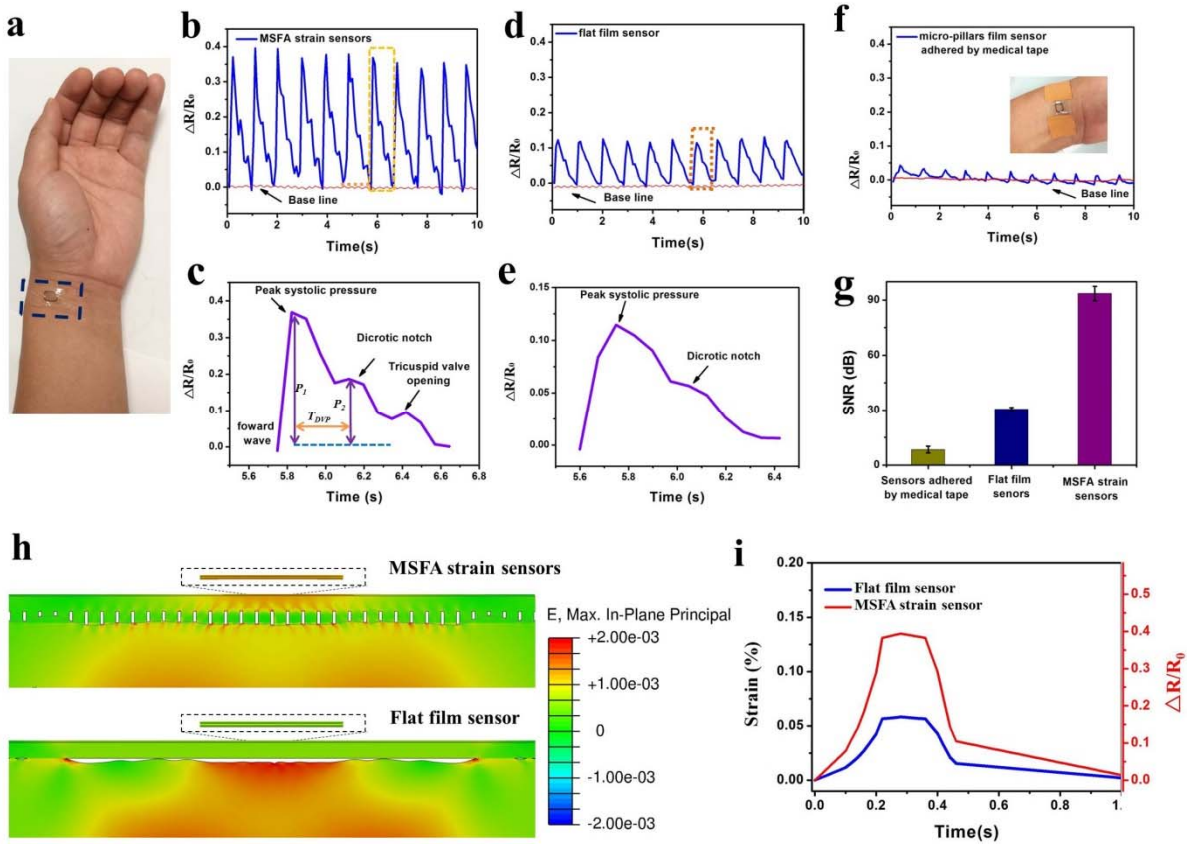

Figure 4 Output signals of the MSFA strain sensors mounted onto the radial artery of the wrist. (a) An MSFA strain sensor adhered to the wrist. Artery pulse signals of a flexible strain sensor with an

MSFA layer (b,c), with a flat fibroin adhesive layer(d,e), and with only the PDMS micro-pillar structure (without the fibroin adhesive layer) attached by a medical tape (f). Inset: the photo of a sensor attached on wrist by a commercial medical tape. Signals from the sensor with the MSFA clearly reflected discernible stages and abundant detailed medical information owing to its high sensitivity. (g) SNR comparison of flexible strain sensors with an MSFA layer, a flat fibroin adhesive layer, and only the PDMS micro-pillar structure. Simulation strain of the strain sensor with an MSFA layer and with a flat fibroin adhesive layer adhered on the wrist, the figures show the typical strain profile at 0.3 s of one cardiac cycle (h) and peak strain value for one cardiac cycle (i). The MSFA strain sensor exhibited much larger strain changes than the sensor with a flat fibroin adhesive layer, leading to high sensitivity.

The MSFA strain sensor not only can be worn on the skin surface without any adhesive taps, but also illustrated ultra-high sensitivity when it was on the wrist of a male volunteer for measuring theartery pulse (Figure 4a). The signals from the sensor exhibited well identified detailed medical information within one pulse, including forward wave, peak systolic pressure, dicrotic notch, and tricuspid valve opening (Figure 4b,c). [53-54] The high sensitivity of the sensor is mainly due to the perfected bonding between the MSFA layer and human skin and the high skin compliance and flexibility. When a flat fibroin adhesive layer without any structure was used, the artery signals amplitude were only one third of the signals from the sensor with the MSFA layer (Figure 4d,e). Additionally, some important details were lost in the signal output, such as the peak representing tricuspid valve opening (Figure 4e). When we bonded the same sensor on the wrist with the PDMS micro-pillar structure using a commercial medical tape, only very small signal output was recorded, i.e. the weak transformation of the wrist skin deformation to the sensor resulting from the poor adhesion between the wrist skin and the sensor (Figure 4f). The signal-to-noise ratio (SNR) was defined as[41]: $SNR = avg(\Delta R_{max}/\sigma_{baseline})$, where $avg(\Delta R_{max})$ is the average resistance change of the maximum radial pulse, $\sigma_{baseline}$ is the standard deviation of the baseline signal without strain. The signal-to-noise ratio (SNR) of the flexible strain sensor with MSFA layer (93.5) is much higher than

the SNRs of the same sensor without the fibroin adhesive (8.4) or with a flat fibroin adhesive layer (30.5) (Figure 4g). The SNR depends on the strain transmission from the deformed skin surface to the sensor. For the sensor bonded by a medical tape at both ends, there may be a lot of small void or air bubble between the skin surface and sensor due to the roughness of the skin surface. These gaps can lead to the loss of the strain signal from the skin surface and therefore a very low SNR. Even if the sensor coated with a flat layer of silk fibroin protein can adhere to the skin surface, the rough skin surface can also lead to a poor surface contact. Therefore, the strain signal may still not be able to transmit to the sensor effectively. On the contrary, the MSFA can adhere to the rough skin surface seamlessly. So the strain signal from the deformation of the skin could be effectively transferred to the sensor, which significantly increases the SNR of the MSFA strain sensor.

To investigate the mechanism of the superior behavior of the MSFA, a Finite Element model was established to simulate the sensor response on pulse cycle. Strain distribution of the micro-pillars/flat sensors was visualized at pulse peak instance (Figure 4h), and peak strain value was evaluated and plotted within one cardiac cycle for both sensors (Figure 4i). The flat fibroin film sensor had a much lower strain since the skin deformation cannot be transferred well to the sensor as the flat film was not conformal for rough skin. On the contrary, the micro-structured fibroin film could be well conformal for the rough skin and was able to attach on the skin surface seamlessly, which effectively transferred the deformation of skin to the sensor deployed. In the one cardiac cycle, the micro-pillar sensor also showed much higher strain changes and resistance changes (more than two times) than the flat film sensor.

2.5. The stable output signals from MSFA strain sensors and their reused performances

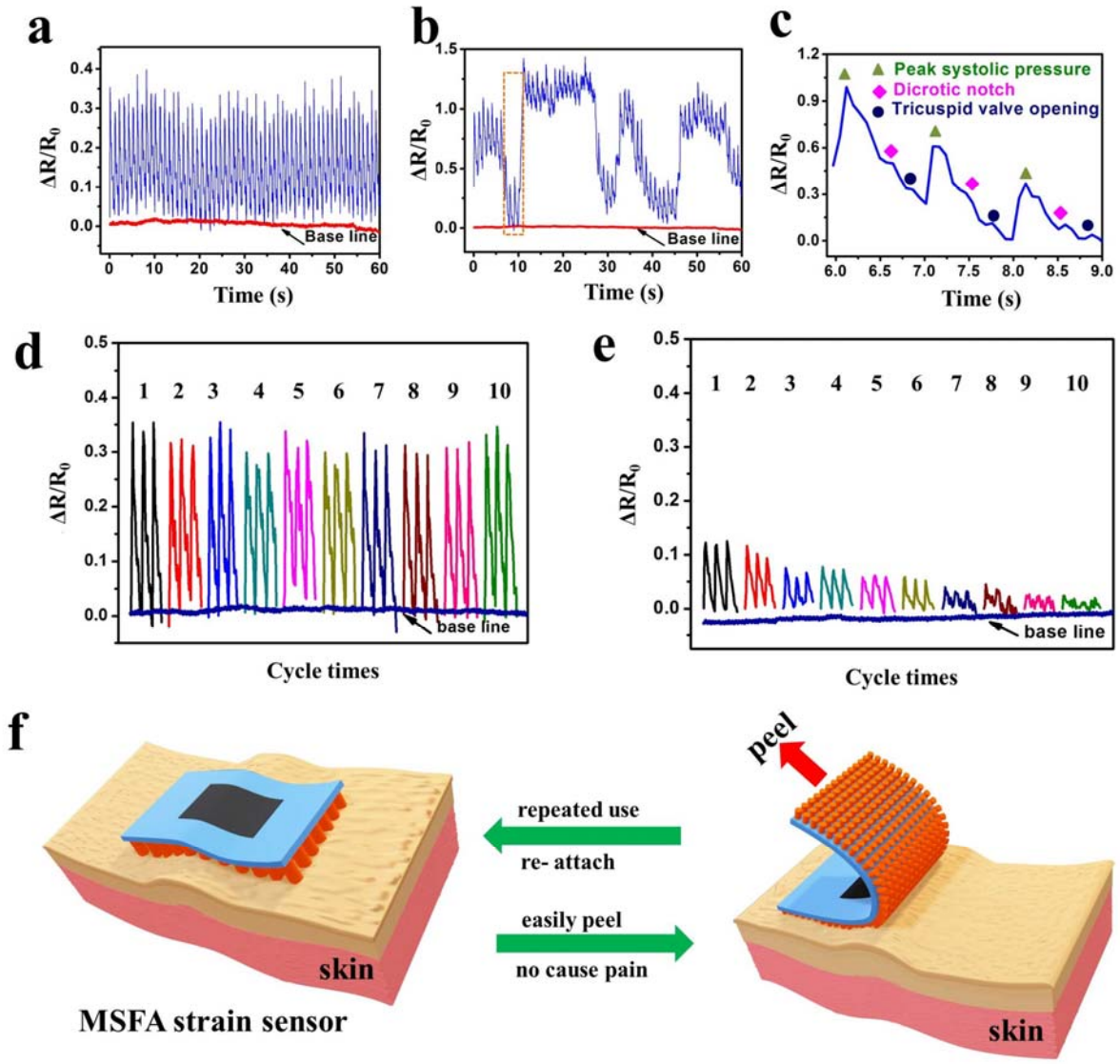

Figure 5 Output signals of an MSFA strain sensor adhered onto the arteria radialis of the wrist (a) in static condition, (b) and (c)(enlarged signal) when turned wrist from the MSFA sensor. The MSFA strain sensor showed stable output signals under static condition, and can also show discernible stages and abundant medical details. Output pulses signals of (d) MSFA strain sensor and (e) a strain sensor with a flat fibroin adhesive film in 10 repeating measurements. The signal from the MSFA strain sensor showed excellent stability during the repeating measurements, whereas the signal from the sensor with a flat fibroin adhesive film significantly deteriorated during the process. (f) Schematic illustration shows that the MSFA strain sensor can be easily peeled off from and re-attached to the skin for repeating use.

The MSFA strain sensor outputted extremely stable signals in static state (Figure 5a) when was bonded onto the skin surface of wrist. During the wrist turning, the signals from the sensor still very clearly showed for each pulse (Figure 5b,c). More importantly, although there were changes in the base resistance of the sensor under large straining conditions, the medical details still could be found in the pulse signal, such as peak systolic pressure, discrotic notch, and tricuspid valve opening (Figure 5c). Such details were completely lost in the signal recorded for the sensor without the MSFA layer (Figure S10).

The reusability of the epidermal sensors is also an important concern since it can greatly reduce cost in daily health monitoring. However, for many flexible epidermal sensors, the reusability is inadequate due to either the deterioration of the adhesives or the damage of the sensor itself during the removing of the sensors. With moderate adhesion and easy peeling-off, our developed MSFA provides excellent reusability (Figure 5f). We have performed continuously measurement of pulse signal on the wrist using the MSFA strain sensor. When re-wearing the sensor after peeling off the sensor from the wrist, the output signals of the MSFA strain sensor showed no perceptible attenuation even after ten repeating adhering-peeling off cycles (Figure 5d and Figure S11). In comparison, the output signals of the sensor with a flat fibroin adhesive layer showed significant attenuation after each repeating cycle (Figure 5e and Figure S11), and almost no meaningful signal after 10 repeating cycles due to the deterioration of the adhesive layer. Such a large decrease of the output signals of the sensor is likely due to the decrease of adhesion force between the flat fibroin adhesive layer and the skin surface after repeated use (Figure 2d). In contrast, the adhesion force of MSFA showed superior durability after 10 cycles due to the microstructure, which insured stable output signals for the MSFA strain sensor.

CONCLUSIONS

In conclusion, we developed a natural silk fibroin protein based, micro-structured adhesive for applications in wearable electronic devices. The MSFA is highly biocompatible and conformable with strong and tunable adhesion on human skin surfaces, and is highly effective even in humid and

wet conditions. The adhesion of MSFA can be finely tuned to avoid the shape pain during the removal process, which is a common problem for all current medical adhesive tapes. The excellent adhesive properties and reusability of the MSFA make it a great adhesive candidate for various epidemic sensor and device applications, such as pulse, body temperature, or chemical sensors. The MSFA can also be used as adhesives for people with sensitive skins and athletes.

4. EXPERIMENTAL SECTION

Fabrication of micro-structured fibroin adhesives (MSFAs). The fabrication process of micro-structured fibroin adhesives is illustrated in Figure 1. The purification of silk fibroin protein has been reported previously.[44] A PDMS micro-pillar film was coated with silk fibroin solution. The PDMS micro-pillar film (micro-pillars side) was treated with oxygen plasma for 5 minutes (pressure of 5 mbar, 80 W), and then immersed into the fibroin solution for 30 s, then spun with a speed of 700 rpm for 60 s using a spin coater. Finally, the micro-pillars film was put into a glass petri dishes and dried in fume hoods for overnight evaporation of formic acid, resulting a micro-structured fibroin adhesive (MSFA) layer.

Adhesion force and peeling force test. The adhesion force and peeling forces tests were performed using a mechanical tester (C42, MTS Systems Corporation). The samples were pre-placed into a chamber with controlled ~ 55% humidity using saturated salt solution (NaBr) overnight. The test environmental humidity was ~55%, measured by a commercial humidity meter HI 9565 (HANNA Instruments). The adhesion forces were measured between a spherical glass disk (R = 50 mm) and the samples (Figure S3a). During a test, the glass disk was moving at a speed of 2 mm/min. After reaching the pre-set compression force, the glass disk would retract from the sample. The adhesion force was defined as the largest negative force measured during the separation process. In the 180^{o} peeling force measurement, the fibroin coated PDMS film sample was adhered onto a PET film, and then kept in a chamber with controlled ~55% humidity overnight. During the test, one the end of the PET film was fixed on one clamp, the one end of the fibroin coated PDMS film was clipped

onto another clamp fixed on the load cell (Figure S3c). The 180º peeling forces between the PET film and different samples were measured at a speed of 5 mm/min.

Fabrication of MSFA strain sensors. The fabrication process of flexible micro-structured fibroin adhesive strain sensor (MSFA strain sensor) is illustrated in Figure S1. A thin single wall carbon nanotubes (P3-SWCNT, containing 1.0-3.0 atomic% carboxylic acid, Carbon Solutions Inc.) layer was used as a conductive layer on the PDMS micro-pillar film. SWCNT solution (1.0 mg/mL) was prepared by dispersing SWCNT in de-ionized water with ultrasonic treatment (Fisher Scientific FB15051) for 3 days, and placed for~24 h to remove large agglomerates. The side of the PDMS micro-pillar film without the micro-pillar structure was covered by a mask with a hollow rectangle (0.6 cm *0.8 cm) followed by oxygen plasma treatment (pressure of 5 mbar, 50 W and 1.0 minutes) to increase the hydrophilicity of the PDMS surface. 20 μL supernatant solution of the SWCNT solution was dropped onto the hydrophilic PDMS surface, and dried in room temperature. Finally, the SWCNT treated PDMS micro-pillar film was coated with silk fibroin as described to form the MSFA strain sensor.

Synchronous electro-mechanical characterization. Copper wires were glued to the two ends of the SWCNT layer using liquid metal (Gallium-indium eutectic, Aldrich). The coppers wires were then connected to a Keithley 4200-SCS for resistance measurement. Tensile machine (C42, MTS Systems Corporation) was employed during the tests at speed of 1 mm/min. To achieve stable electrical performance, all the electro-mechanical testing was conducted after 200 cycles as microcrack pattern in the SWCNT network would become stable after warm-up cycles (usually 50-200 cycles).

Strain distribution from FEM simulation. Numerical models adopting Finite Element Method (FEM) were established to investigate the sensitivity of sensor in this study. The FEM models with and without micro-pillar were built up using commercial software ABAQUS (schematically shown in support Figure **10**). Since the cross section of wrist and sensor device is approximately uniform along the length direction of the sensor device, plane strain 2D models were used in this study for minimized the computational cost with better approximation. To evaluate the effect of skin surface

roughness, the skin surface geometry profile was modeled using real scan data. The bottom of the sensor was placed upon the skin surface. The sensor with micro-pillar was assumed to make a full contact with the skin surface, while the flat device was assumed to make contact with the highest crests of the skin surface. The model was meshed using ~66K linear quadrilateral elements for the both device and skin, and ~400 beam elements were used to model the carbon nanotube sensor. The material parameters of PDMS was in-house measured through a simple tension, and calibrated with hyperelastic material (Mooney–Rivlin model with C10=0.25484MPa, C01=0.06371MPa, D1=0.006283MPa^{-1}), while the skin was simulated using linear elastic material model with parameters selected according to Ref.[55] with E = 0.6MPa and $\nu = 0.4$. Material interface was simulated through a direct tie of different regions with different material parameters. To simulate the effect of pulse cycle, the pressure was applied on the bottom center in the model, while the other area of the bottom was fixed in all directions, to mimic the effect of muscle constrain on the skin. The applied pressure was calibrated, so the maximum height caused by pulse was the same as experimental measurement, i.e. $31\mu m$.[56] Based on above settings in the FEM models, one cycle of pulse =1.1 second was simulated using implicit dynamic FEM, which was same as the experimental testing. The strain output from the beam elements was treated as the strain measurement of sensor on the PDMS surface. Mesh convergence was checked and observed in this FEM model.

ASSOCIATED CONTENT

Supporting Information

Supplementary Methods: fabrication micro-pillars, pulse measurement. Supplementary Figures S1−S12: optical microscope images of micro-pillars and fibroin coated PDMS miciro-pillars, SEM of silk fibroin coated micro-pillars, the photos of measurement equipment, adhesion energy of PDMS micro-pillars, the peeling forces of different materials, microscopic image and roughness of skin replica, photos of peeling an MSFA and a medical tape, the performance of the MSFA and medical tape in wet conditions, the biocompatibility the MSFA, illustration of the fabrication method, the characterization of SWCNTs ring in the sensor, output signals and enlarged signals of a strain sensor with a flat fibroin, the signal-to-noise ratio (SNR) of a flexible strain sensor, schematics on the modeling detail and boundary conditions. Supplementary movie S1-3: strong adhesion, peeling from skin, adhesion in wet conditions.

AUTHOR INFORMATION

Corresponding Author

***E-mail:** liuzj@ihpc.a-star.edu.sg (Z. Liu)

***E-mail:** chenxd@ntu.edu.sg (X. Chen)

***E-mail:** yujing@ntu.edu.sg (J. Yu)

Conflict of Interest

The authors declare no conflict of interest.

ACKNOWLEDGMENTS

X.J.L thanks Singapore Ministry of Education Academic Research Fund Tier 1 (RG-94/18). J.L.W., J.L., Z.J.L, X.D.C., and J.Y. acknowledge the AME programmatic funding scheme of Cyber Physiochemical Interfaces (CPI) project #A18A1b0045.

REFERENCES

(1) Chortos, A.; Liu, J.; Bao, Z. Pursuing Prosthetic Electronic Skin. *Nat. Mater.* **2016,** *15*, 937-950.

(2) Ma, Y.; Feng, X.; Rogers, J. A.; Huang, Y.; Zhang, Y. Design and Application of 'J-Shaped' Stress-Strain Behavior in Stretchable Electronics: A Review. *Lab Chip* **2017,** *17*, 1689-1704.

(3) Rogers, J. A.; Someya, T.; Huang, Y. Materials and Mechanics for Stretchable Electronics. *Science* **2010,** *327*, 1603-1607.

(4) Kim, D. H.; Lu, N.; Ma, R.; Kim, Y. S.; Kim, R. H.; Wang, S.; Wu, J.; Won, S. M.; Tao, H.; Islam, A.; Yu, K. J.; Kim, T. I.; Chowdhury, R.; Ying, M.; Xu, L.; Li, M.; Chung, H. J.; Keum, H.; McCormick, M.; Liu, P.; Zhang, Y. W.; Omenetto, F. G.; Huang, Y.; Coleman, T.; Rogers, J. A. Epidermal Electronics. *Science* **2011,** *333*, 838-843.

(5) Imani, S.; Bandodkar, A. J.; Mohan, A. M.; Kumar, R.; Yu, S.; Wang, J.; Mercier, P. P. A Wearable Chemical-Electrophysiological Hybrid Biosensing System for Real-Time Health and Fitness Monitoring. *Nat. Commun.* **2016,** *7*, 11650.

(6) Hong, Y. J.; Jeong, H.; Cho, K. W.; Lu, N.; Kim, D. H. Wearable and Implantable Devices for Cardiovascular Healthcare: From Monitoring to Therapy Based on Flexible and Stretchable Electronics. *Adv. Funct. Mater.* **2019,** *29*, 1808247.

(7) Zhang, Y.; Huang, Y.; Rogers, J. A. Mechanics of Stretchable Batteries and Supercapacitors. *Curr. Opin. Solid State Mater. Sci.* **2015,** *19*, 190-199.

(8) Boutry, C. M.; Beker, L.; Kaizawa, Y.; Vassos, C.; Tran, H.; Hinckley, A. C.; Pfattner, R.; Niu, S.; Li, J.; Claverie, J.; Wang, Z.; Chang, J.; Fox, P. M.; Bao, Z. Biodegradable and Flexible Arterial-Pulse Sensor for the Wireless Monitoring of Blood Flow. *Nat. Biomed. Eng.* **2019,** *3*, 47-57.

(9) Gao, L.; Zhu, C.; Li, L.; Zhang, C.; Liu, J.; Yu, H. D.; Huang, W. All Paper-Based Flexible and Wearable Piezoresistive Pressure Sensor. *ACS Appl. Mater. Interfaces* **2019,** *11*, 25034-25042.

(10) Yetisen, A. K.; Martinez-Hurtado, J. L.; Unal, B.; Khademhosseini, A.; Butt, H. Wearables in Medicine. *Adv. Mater.* **2018,** *30*, 1706910.

(11) Chung, H. U.; Kim, B. H.; Lee, J. Y.; Lee, J.; Xie, Z.; Ibler, E. M.; Lee, K.; Banks, A.; Jeong, J. Y.; Kim, J.; Ogle, C.; Grande, D.; Yu, Y.; Jang, H.; Assem, P.; Ryu, D.; Kwak, J. W.; Namkoong, M.; Park, J. B.; Lee, Y.; Kim, D. H.; Ryu, A.; Jeong, J.; You, K.; Ji, B.; Liu, Z.; Huo, Q.; Feng, X.; Deng, Y.; Xu, Y.; Jang, K. I.; Kim, J.; Zhang, Y.; Ghaffari, R.; Rand, C. M.; Schau, M.; Hamvas, A.; Weese-Mayer, D. E.; Huang, Y.; Lee, S. M.; Lee, C. H.; Shanbhag, N. R.; Paller, A. S.; Xu, S.; Rogers, J. A. Binodal, Wireless Epidermal Electronic Systems with in-Sensor Analytics for Neonatal Intensive Care. *Science* **2019,** *363*, eaau0780.

(12) Sugiyama, M.; Uemura, T.; Kondo, M.; Akiyama, M.; Namba, N.; Yoshimoto, S.; Noda, Y.; Araki, T.; Sekitani, T. An Ultraflexible Organic Differential Amplifier for Recording Electrocardiograms. *Nat. Electron.* **2019,** *2*, 351-360.

(13) Jin, H.; Nayeem, M. O. G.; Lee, S.; Matsuhisa, N.; Inoue, D.; Yokota, T.; Hashizume, D.; Someya, T. Highly Durable Nanofiber-Reinforced Elastic Conductors for Skin-Tight Electronic Textiles. *ACS Nano* **2019,** *13*, 7905-7912.

(14) Wang, C.; Xia, K.; Wang, H.; Liang, X.; Yin, Z.; Zhang, Y. Advanced Carbon for Flexible and Wearable Electronics. *Adv. Mater.* **2019,** *31*, 1801072.

(15) Matsuhisa, N.; Chen, X.; Bao, Z.; Someya, T. Materials and Structural Designs of Stretchable Conductors. *Chem. Soc. Rev.* **2019,** *48*, 2946-2966.

(16) Choi, S.; Han, S. I.; Jung, D.; Hwang, H. J.; Lim, C.; Bae, S.; Park, O. K.; Tschabrunn, C. M.; Lee, M.; Bae, S. Y.; Yu, J. W.; Ryu, J. H.; Lee, S. W.; Park, K.; Kang, P. M.; Lee, W. B.; Nezafat, R.; Hyeon, T.; Kim, D. H. Highly Conductive, Stretchable and Biocompatible Ag-Au Core-Sheath Nanowire Composite for Wearable and Implantable Bioelectronics. *Nat. Nanotechnol.* **2018,** *13*, 1048-1056.

(17) Wang, S.; Oh, J. Y.; Xu, J.; Tran, H.; Bao, Z. Skin-Inspired Electronics: An Emerging Paradigm. *Acc. Chem. Res.* **2018,** *51*, 1033-1045.

(18) Jayathilaka, W.; Qi, K.; Qin, Y.; Chinnappan, A.; Serrano-Garcia, W.; Baskar, C.; Wang, H.; He, J.; Cui, S.; Thomas, S. W.; Ramakrishna, S. Significance of Nanomaterials in Wearables: A Review on Wearable Actuators and Sensors. *Adv. Mater.* **2019,** *31*, 1805921.

(19) Hua, Q.; Sun, J.; Liu, H.; Bao, R.; Yu, R.; Zhai, J.; Pan, C.; Wang, Z. L. Skin-Inspired Highly Stretchable and Conformable Matrix Networks for Multifunctional Sensing. *Nat. Commun.* **2018,** *9*, 244.

(20) An, B. W.; Heo, S.; Ji, S.; Bien, F.; Park, J. U. Transparent and Flexible Fingerprint Sensor Array with Multiplexed Detection of Tactile Pressure and Skin Temperature. *Nat. Commun.* **2018,** *9*, 2458.

(21) Kim, Y.; Chortos, A.; Xu, W.; Liu, Y.; Oh, J. Y.; Son, D.; Kang, J.; Foudeh, A. M.; Zhu, C.; Lee, Y.; Niu, S.; Liu, J.; Pfattner, R.; Bao, Z.; Lee, T. W. A Bioinspired Flexible Organic Artificial Afferent Nerve. *Science* **2018,** *360*, 998-1003.

(22) Kang, S. K.; Koo, J.; Lee, Y. K.; Rogers, J. A. Advanced Materials and Devices for Bioresorbable Electronics. *Acc. Chem. Res.* **2018,** *51*, 988-998.

(23) Huang, K. H.; Tan, F.; Wang, T. D.; Yang, Y. J. A Highly Sensitive Pressure-Sensing Array for Blood Pressure Estimation Assisted by Machine-Learning Techniques. *Sensors* **2019,** *19*, 848.

(24) Amjadi, M.; Kyung, K.-U.; Park, I.; Sitti, M. Stretchable, Skin-Mountable, and Wearable Strain Sensors and Their Potential Applications: A Review. *Adv. Funct. Mater.* **2016,** *26*, 1678-1698.

(25) Yao, S.; Swetha, P.; Zhu, Y. Nanomaterial-Enabled Wearable Sensors for Healthcare. *Adv Healthc Mater* **2018,** *7*, 1700889.

(26) Yang, Y.; Song, X.; Li, X.; Chen, Z.; Zhou, C.; Zhou, Q.; Chen, Y. Recent Progress in Biomimetic Additive Manufacturing Technology: From Materials to Functional Structures. *Adv. Mater.* **2018,** *30*, 1706539.

(27) Gong, S.; Yap, L. W.; Zhu, B.; Cheng, W. Multiscale Soft-Hard Interface Design for Flexible Hybrid Electronics. *Adv. Mater.* **2019**, 1902278. https://doi.org/10.1002/adma.201902278.

(28) Wolf, M. P.; Salieb-Beugelaar, G. B.; Hunziker, P. Pdms with Designer Functionalities—Properties, Modifications Strategies, and Applications. *Prog. Polym. Sci.* **2018,** *83*, 97-134.

(29) Baik, S.; Kim, D. W.; Park, Y.; Lee, T. J.; Ho Bhang, S.; Pang, C. A Wet-Tolerant Adhesive Patch Inspired by Protuberances in Suction Cups of Octopi. *Nature* **2017,** *546*, 396-400.

(30) Zhao, Y.; Wu, Y.; Wang, L.; Zhang, M.; Chen, X.; Liu, M.; Fan, J.; Liu, J.; Zhou, F.; Wang, Z. Bio-Inspired Reversible Underwater Adhesive. *Nat. Commun.* **2017,** *8*, 2218.

(31) Singla, S.; Amarpuri, G.; Dhopatkar, N.; Blackledge, T. A.; Dhinojwala, A. Hygroscopic Compounds in Spider Aggregate Glue Remove Interfacial Water to Maintain Adhesion in Humid Conditions. *Nat. Commun.* **2018,** *9*, 1890.

(32) O'Connor, R. J.; Ogle, J.; Odio, M. Induction of Epidermal Damage by Tape Stripping to Evaluate Skin Mildness of Cleansing Regimens for the Premature Epidermal Barrier. *Int. J. Dermatol.* **2016,** *55 Suppl 1*, 21-27.

(33) Wang, D.; Xu, H.; Chen, S.; Lou, X.; Tan, J.; Xu, Y. Medical Adhesive-Related Skin Injuries and Associated Risk Factors in a Pediatric Intensive Care Unit. *Adv. Skin Wound Care* **2019,** *32*, 176-182.

(34) Gan, D.; Xing, W.; Jiang, L.; Fang, J.; Zhao, C.; Ren, F.; Fang, L.; Wang, K.; Lu, X. Plant-Inspired Adhesive and Tough Hydrogel Based on Ag-Lignin Nanoparticles-Triggered Dynamic Redox Catechol Chemistry. *Nat. Commun.* **2019,** *10*, 1487.

(35) Lee, H.; Lee, B. P.; Messersmith, P. B. A Reversible Wet/Dry Adhesive Inspired by Mussels and Geckos. *Nature* **2007,** *448*, 338-341.

(36) Baik, S.; Lee, H. J.; Kim, D. W.; Kim, J. W.; Lee, Y.; Pang, C. Bioinspired Adhesive Architectures: From Skin Patch to Integrated Bioelectronics. *Adv. Mater.* **2019,** *31*, 1803309.

(37) Hu, H.; Tian, H.; Shao, J.; Li, X.; Wang, Y.; Wang, Y.; Tian, Y.; Lu, B. Discretely Supported Dry Adhesive Film Inspired by Biological Bending Behavior for Enhanced Performance on a Rough Surface. *ACS Appl. Mater. Interfaces* **2017,** *9*, 7752-7760.

(38) Bae, W. G.; Kim, D.; Kwak, M. K.; Ha, L.; Kang, S. M.; Suh, K. Y. Enhanced Skin Adhesive Patch with Modulus-Tunable Composite Micropillars. *Adv. Healthc. Mater.* **2013,** *2*, 109-113.

(39) Park, J.; Sohn, J.; Cho, D.; Jeon, S.; Kim, T. Bioinspired, Highly Stretchable, and Conductive Dry Adhesives Based on 1d–2d Hybrid Carbon Nanocomposites for All-in-One Ecg Electrodes. *ACS Nano* **2016,** *10*, 4770-4778.

(40) Liu, Y.; He, K.; Chen, G.; Leow, W. R.; Chen, X. Nature-Inspired Structural Materials for Flexible Electronic Devices. *Chem. Rev.* **2017,** *117*, 12893-12941.

(41) Pang, C.; Koo, J. H.; Nguyen, A.; Caves, J. M.; Kim, M. G.; Chortos, A.; Kim, K.; Wang, P. J.; Tok, J. B.; Bao, Z. Highly Skin-Conformal Microhairy Sensor for Pulse Signal Amplification. *Adv. Mater.* **2015,** *27*, 634-640.

(42) Drotlef, D. M.; Amjadi, M.; Yunusa, M.; Sitti, M. Bioinspired Composite Microfibers for Skin Adhesion and Signal Amplification of Wearable Sensors. *Adv. Mater.* **2017,** *29*, 1701353.

(43) Huang, W.; Ling, S.; Li, C.; Omenetto, F. G.; Kaplan, D. L. Silkworm Silk-Based Materials and Devices Generated Using Bio-Nanotechnology. *Chem. Soc. Rev.* **2018,** *47*, 6486-6504.

(44) Chen, G.; Matsuhisa, N.; Liu, Z.; Qi, D.; Cai, P.; Jiang, Y.; Wan, C.; Cui, Y.; Leow, W. R.; Liu, Z.; Gong, S.; Zhang, K. Q.; Cheng, Y.; Chen, X. Plasticizing Silk Protein for on-Skin Stretchable Electrodes. *Adv. Mater.* **2018,** *30*, 1800129.

(45) Kim, D. H.; Viventi, J.; Amsden, J. J.; Xiao, J.; Vigeland, L.; Kim, Y. S.; Blanco, J. A.; Panilaitis, B.; Frechette, E. S.; Contreras, D.; Kaplan, D. L.; Omenetto, F. G.; Huang, Y.; Hwang, K. C.; Zakin, M. R.; Litt, B.; Rogers, J. A. Dissolvable Films of Silk Fibroin for Ultrathin Conformal Bio-Integrated Electronics. *Nat. Mater.* **2010,** *9*, 511-517.

(46) Yu, X.; Shou, W.; Mahajan, B. K.; Huang, X.; Pan, H. Materials, Processes, and Facile Manufacturing for Bioresorbable Electronics: A Review. *Adv. Mater.* **2018,** *30*, 1707624.

(47) Tao, H.; Brenckle, M. A.; Yang, M.; Zhang, J.; Liu, M.; Siebert, S. M.; Averitt, R. D.; Mannoor, M. S.; McAlpine, M. C.; Rogers, J. A.; Kaplan, D. L.; Omenetto, F. G. Silk-Based Conformal, Adhesive, Edible Food Sensors. *Adv. Mater.* **2012,** *24*, 1067-1072.

(48) Seo, J.-W.; Kim, H.; Kim, K.; Choi, S. Q.; Lee, H. J. Calcium-Modified Silk as a Biocompatible and Strong Adhesive for Epidermal Electronics. *Adv. Funct. Mater.* **2018,** *28*, 1800802.

(49) Yucel, T.; Kojic, N.; Leisk, G. G.; Lo, T. J.; Kaplan, D. L. Non-Equilibrium Silk Fibroin Adhesives. *J. Struct. Biol.* **2010,** *170*, 406-412.

(50) Das, S.; Chary, S.; Yu, J.; Tamelier, J.; Turner, K. L.; Israelachvili, J. N. Jkr Theory for the Stick-Slip Peeling and Adhesion Hysteresis of Gecko Mimetic Patterned Surfaces with a Smooth Glass Surface. *Langmuir* **2013,** *29*, 15006-15012.

(51) Johnston, E. R.; Miyagi, Y.; Chuah, J.-A.; Numata, K.; Serban, M. A. Interplay between Silk Fibroin's Structure and Its Adhesive Properties. *Acs Biomater. Sci. Eng.* **2018,** *4*, 2815-2824.

(52) Minoura N.; Tsukada M.; Nagura M. Physico-chemical properties of silk fibroin membrane as a biomaterial. *Biomaterials*, **1990**, *11*, 430-434.

(53) Jiang, Y.; Liu, Z.; Matsuhisa, N.; Qi, D.; Leow, W. R.; Yang, H.; Yu, J.; Chen, G.; Liu, Y.; Wan, C.; Liu, Z.; Chen, X. Auxetic Mechanical Metamaterials to Enhance Sensitivity of Stretchable Strain Sensors. *Adv. Mater.* **2018,** *30*, 1706589.

(54) Choong, C. L.; Shim, M. B.; Lee, B. S.; Jeon, S.; Ko, D. S.; Kang, T. H.; Bae, J.; Lee, S. H.; Byun, K. E.; Im, J.; Jeong, Y. J.; Park, C. E.; Park, J. J.; Chung, U. I. Highly Stretchable Resistive Pressure Sensors Using a Conductive Elastomeric Composite on a Micropyramid Array. *Adv. Mater.* **2014,** *26*, 3451-3458.

(55) Pawlaczyk, M.; Lelonkiewicz, M.; Wieczorowski, M., Age-dependent biomechanical properties of the skin. *Postepy Dermatologii I Alergologii* **2013,** *30*, 302-306.

(56) Chiu, S.-Y.; Wang, C.-H.; Lee, S.-S.; Wu, W.-J.; Hsu, Y.-H.; Lee, C.-K., Measuring the arterial-induced skin vibration by geometrical moiré fringe. In *Optical Diagnostics and Sensing XVIII: Toward Point-of-Care Diagnostics*, **2018,** 10501, 105010H.

TOC

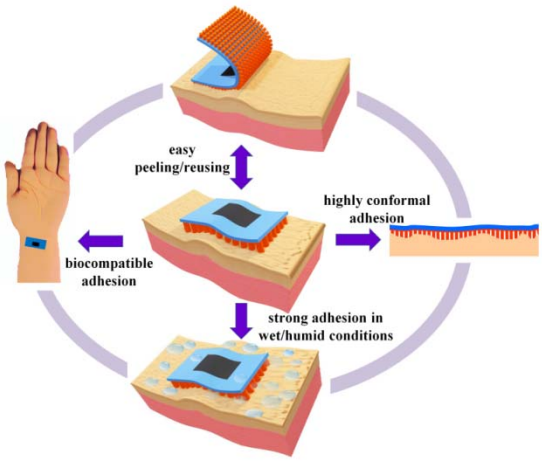
easy
peeling/reusing
highly conformal
adhesion
biocompatible
adhesion
strong adhesion in
wet/humid conditions

Supporting Information

Bio-inspired, Micro-structured Silk Fibroin Adhesives for Flexible Skin Sensors

Xijian Liu,[1,2] Jun Liu,[3] Jilei Wang, [2] Ting Wang,[2] Ying Jiang,[2] Junqing Hu,[4] Zhuangjian Liu[*],[3] Xiaodong Chen,[* 2] Jing Yu[*2]

[1]College of Chemistry and Chemical Engineering, Shanghai University of Engineering Science, Shanghai 201620, P. R. China.

[2]School of Materials Science and Engineering, Nanyang Technological University, 639798, Singapore. E-mail: chenxd@ntu.edu.sg; yujing@ntu.edu.sg

[3]Institute of High Performance Computing, Agency for Science Technology and Research, 1 Fusionopolis Way, 138632, Singapore.

Email: liuzj@ihpc.a-star.edu.sg

[4]College of Health Science and Environmental Engineering, Shenzhen Technology University, Shenzhen, 518118, China.

Supplementary Methods

Fabrication micro-pillars. Silicon wafers were cleaned by nitrogen purging and treatment of oxygen plasma (80 W) at a pressure of 5 mbar for 5 minutes. SU-8 photoresist were coated onto the wafers according the operating instruction of MICRO CHEM for SU-8 to achieve film thicknesses of ~40 μm, 80 μm, and 120 μm, respectively. After soft bake, UV exposure with a mask, post expose bake, developing, rinsing, dry and hard bake (Table S1), the SU-8 patterns were prepared. The SU-8 patterned silicon wafers were further coated with hexadecafluoro-1,1,2,2-tetrahydrooctyltrichlorosilane using chemical vapor deposition by heating the silicon wafers to 180 ^{o}C with 40 μL hexadecafluoro-1,1,2,2-tetrahydrooctyltrichlorosilane in a sealed glass container.

Table S1. The parameters of photoetching

Pillars heights	40 μm	80 μm	120 μm
soft bake temperature (^{o}C)	95	95	95
soft bake time (min)	9	14	20
exposure time (s)	3.5	4.0	4.5
post expose bake (^{o}C)	95	95	95
post expose bake time (min)	8	13	18
developing time (min)	8	15	20

Sylgard 184 prepolymer and crosslinker were mixed at 10: 1 ratio, then poured onto the SU-8 patterned wafers. The wafers were degassed in a vacuum oven for 30 minutes, then spun with speed of 900 rpm for 45 s using a spin coater. The PDMS was cured by baking for 24 h at 60 ^{o}C. Peeling the fully cured PDMS layer from the mold giving a PDMS film with arrays of micro-pillars of different diameters (from 20 to 80 μm) and heights (40, 80 and 120 μm).

Pulse measurement. A MSFA strain sensor was adhered onto the skin surface of the wrist above the radial artery. The output signals of the MSFA strain sensor were recorded. The volunteer is 170 cm height. The signals of MSFA strain sensor clearly showed that the time delay (TDVP) was around 300 ms. Then the derived arterial stiffness index (S.I. = volunteer height/TDVP) is 5.7%, and the reflection index (R.I. = P2/P1 × 100) is 50.6%, which are all in the normal range of a healthy adult.[1-2] SNR was calculated according to previous method: [3]SNR= avg($\Delta R_{max}/\sigma_{baseline}$). Where avg($\Delta R_{max}$) is the average resistance change of the maximum radial pulse, $\sigma_{baseline}$ is the standard deviation of the baseline signal without strain.

Supplementary Images

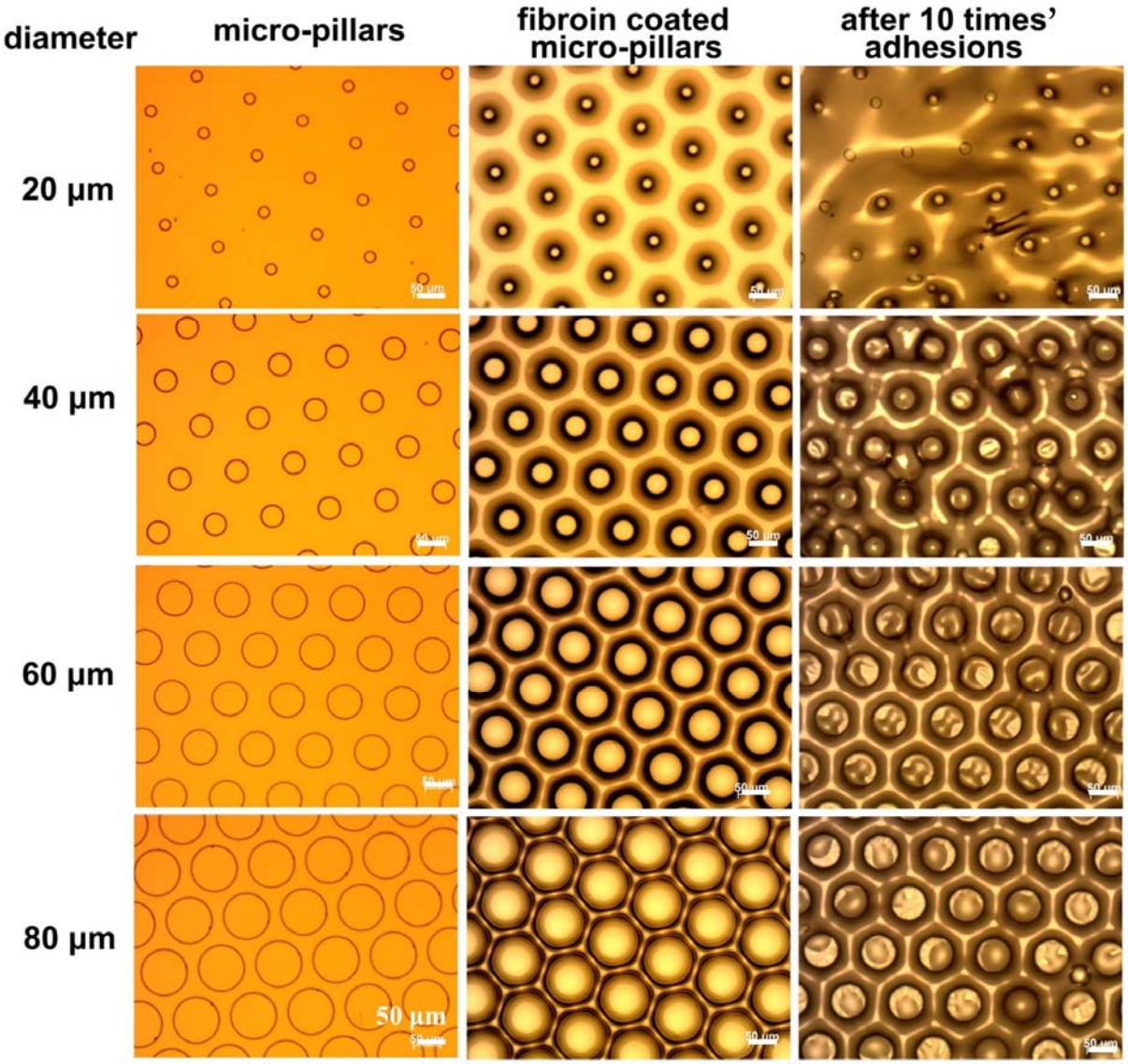

Figure S1 Optical microscope images of micro-pillars and fibroin coated PDMS miciro-pillars with different diameters at height of ~80 μm. Scale bar: 50 μm.

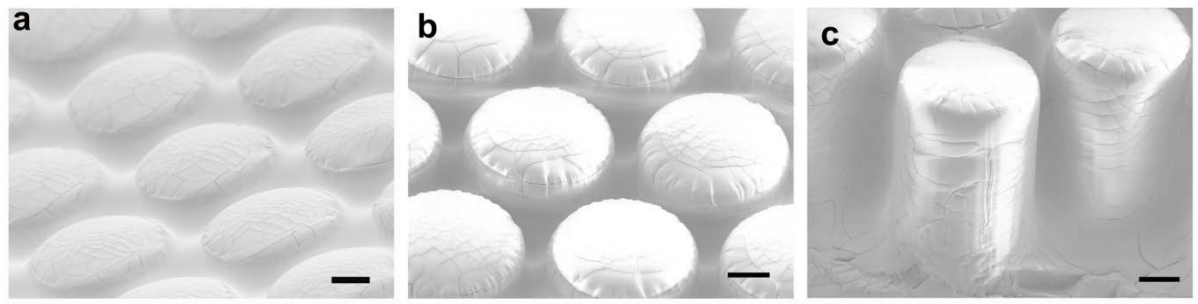

Figure S2 The magnified SEM of silk fibroin coated micro-pillars with diameter of 80 μm at (a) ~40 μm, (b) ~80 μm and (c) ~120 μm height. scale bar:20 μm.

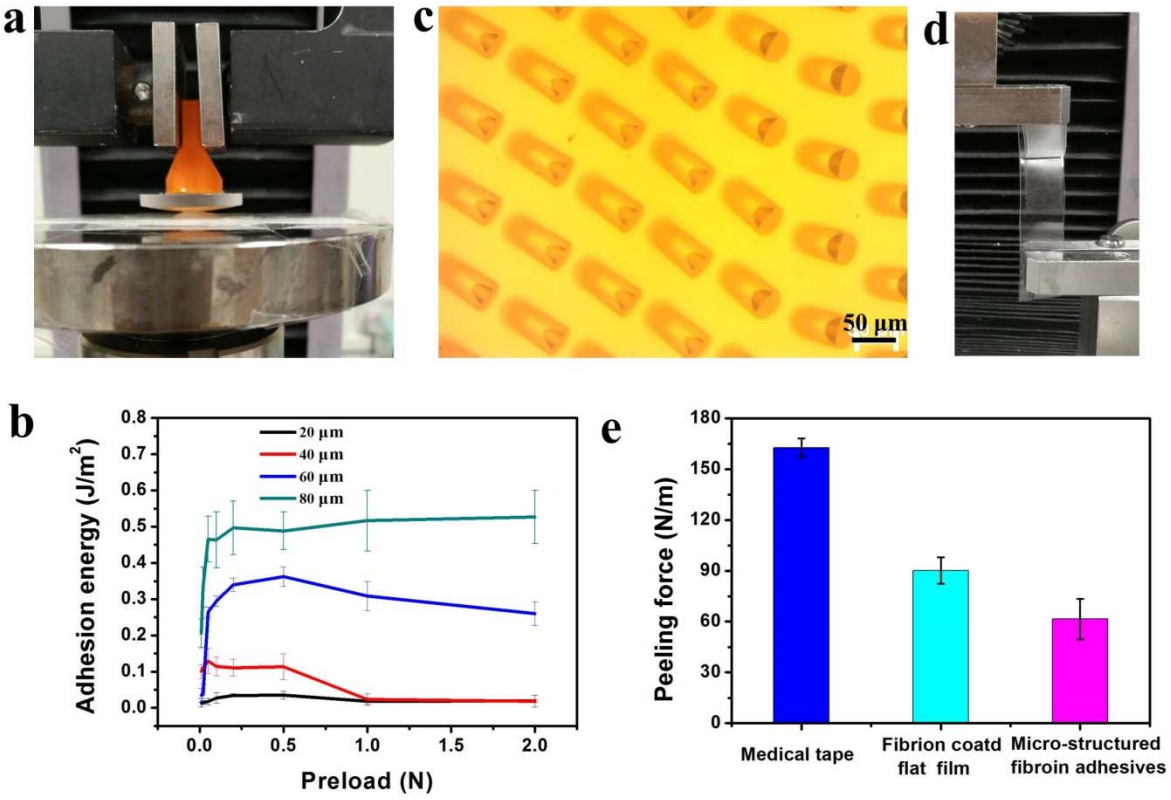

Figure S3 (a) The photo of equipment to measure adhesion energy using the JKR method. (b) Adhesion energy of PDMS micro-pillars with diameter from 20 to 80 μm (80 μm pillar height) under different preload force. (c) The micro-pillar (diameter of 40 μm) under small pressure leads to bend. (d) The photo of peeling forces measurement by MTS. (e)The peeling forces of 180º peeling between a medical tape, a fibroin coated flat film, and an MSFA layer.

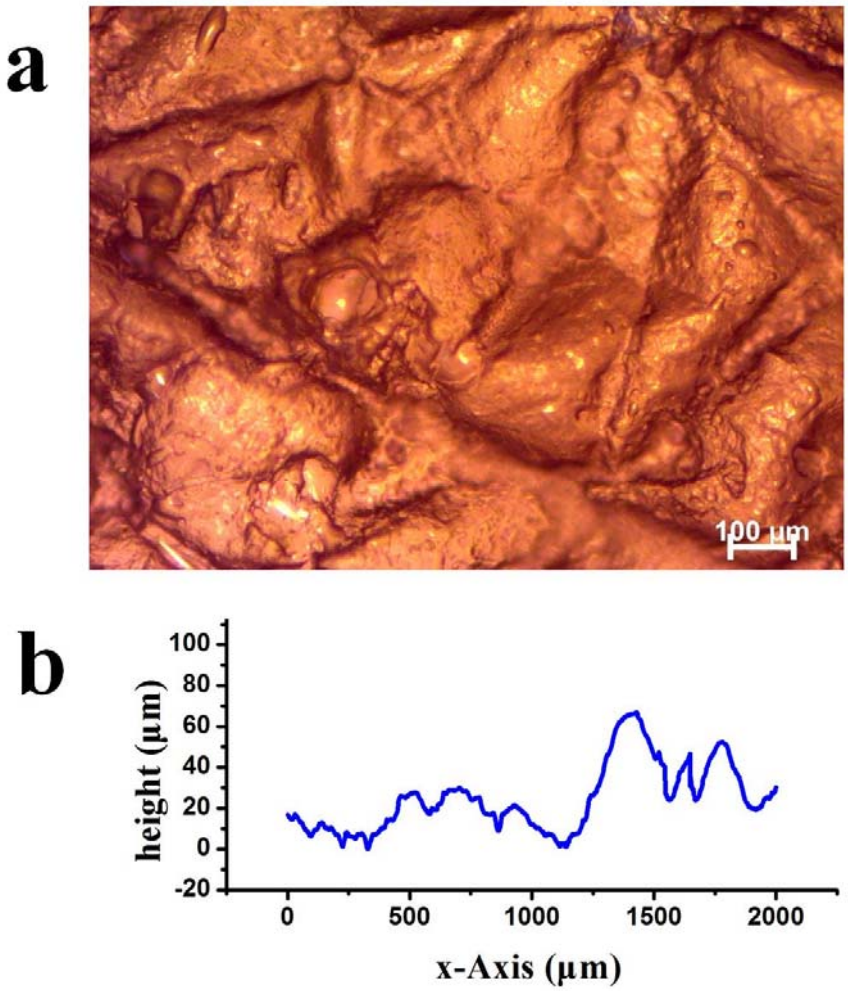

Figure S4 (a) Microscopic image of an artificial PDMS skin replica. (b) The roughness of skin replica scanned by Surface Profiler, showing a vertical roughness of ~70 μm.

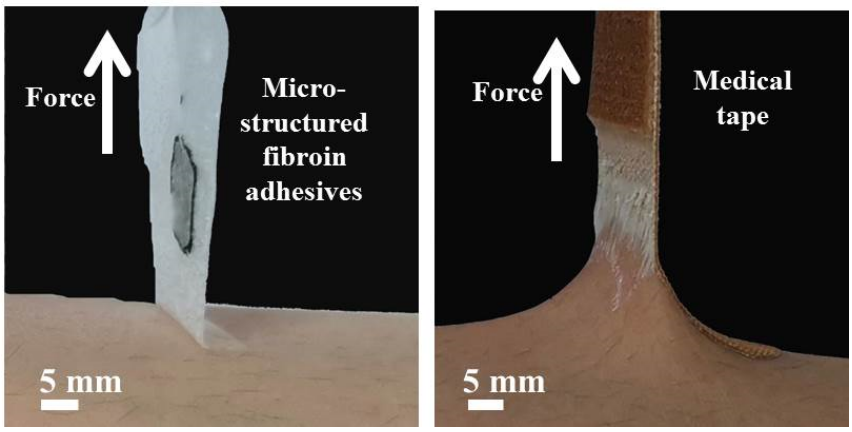

Figure S5 Photos of peeling an MSFA (left) and a medical tape from the arm skin of a healthy adult.

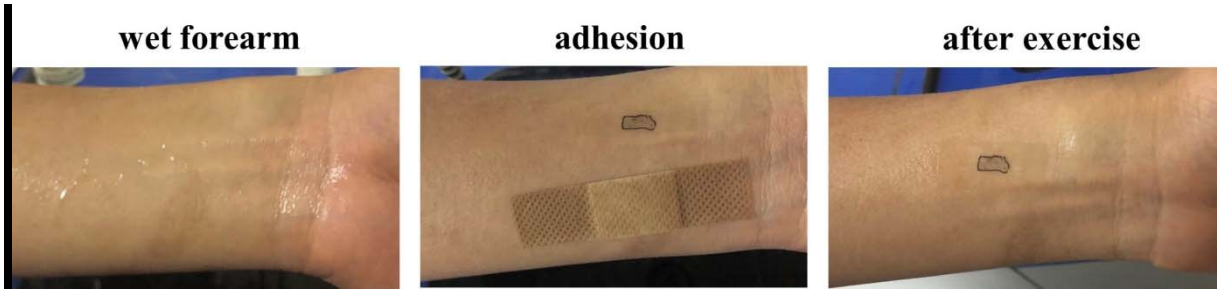

Figure S6 The performance of the MSFA and medical tape in wet conditions. The micro-structured fibroin adhesives and medical tape adhered onto the skin of wet (mixture of sweat and water) forearm, then exercised. The medical tape was detached from skin, however, the MSFA still maintained its adhesion on the skin surface.

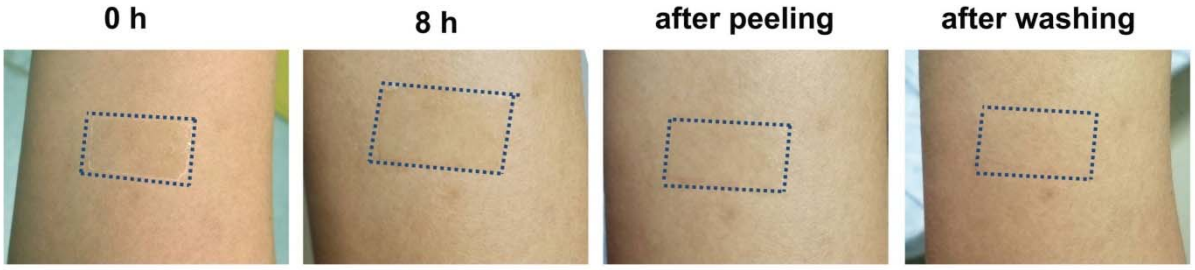

Figure S7 The biocompatibility the MSFA. The MFSA adhered on the skin for 8h (The dotted boxes were the adhesion area of the film). After peeling and washing, the skin showed no difference with the normal skin, demonstrating no hypersensitivity.

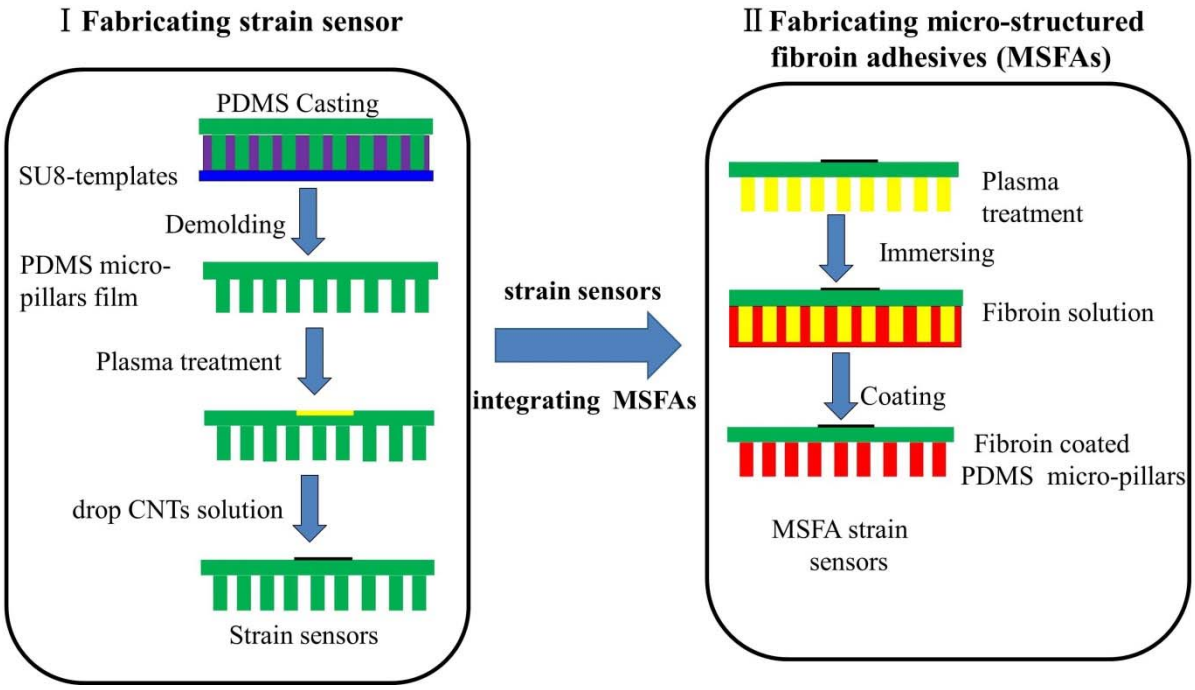

Figure S8 Illustration of the fabrication method for stretchable strain sensors integrated with micro-structured fibroin adhesives.

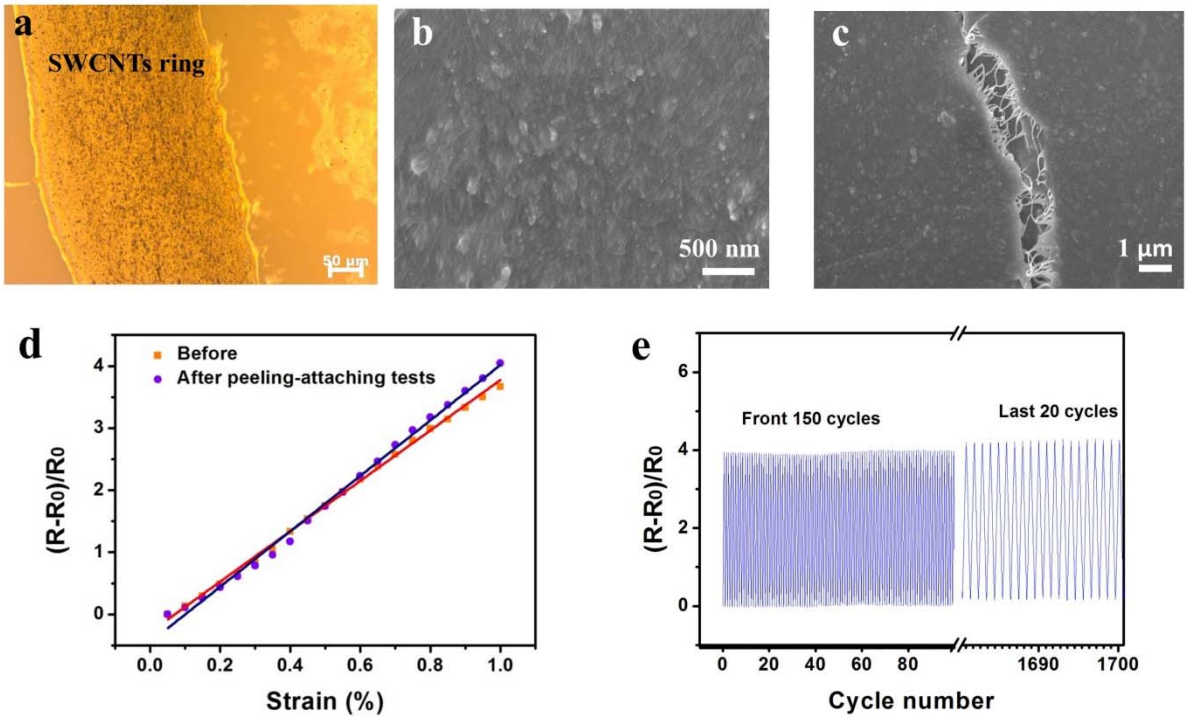

Figure S9 The characterization of SWCNTs ring in the sensor. The microscope images (a) and SEM images (b) of SWCNTS ring before tension. (c)The SEM images of SWCNTs ring under

tension. (d) Normalized resistance change as a function of the strain before and after ten times' repeated peeling-attaching tests. (e) The cyclic durability test of 1700 cycles under 1.0% tensile strain.

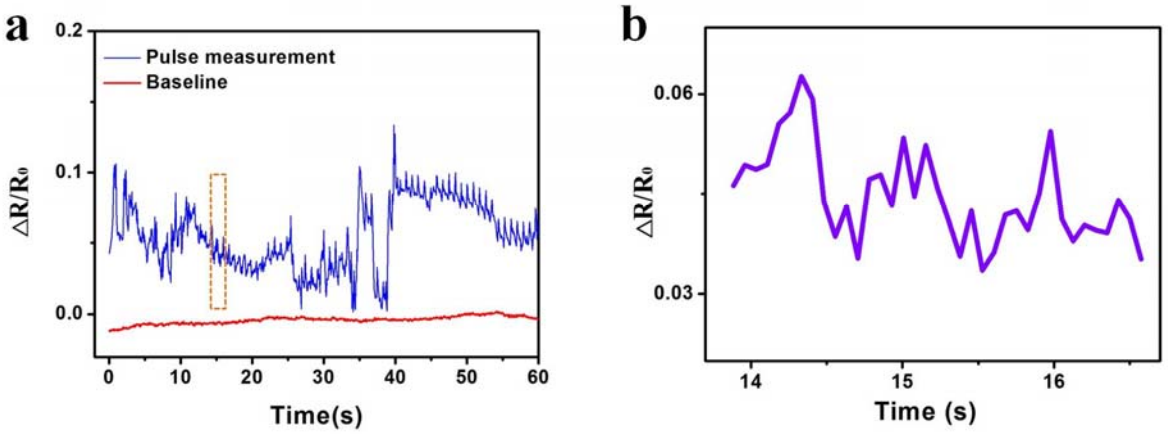

Figure S10 Output signals (a) and enlarged signals (b) of a strain sensor with a flat fibroin adhesive layer adhered onto the skin surface of the wrist near the radial artery during the turning of the wrist.

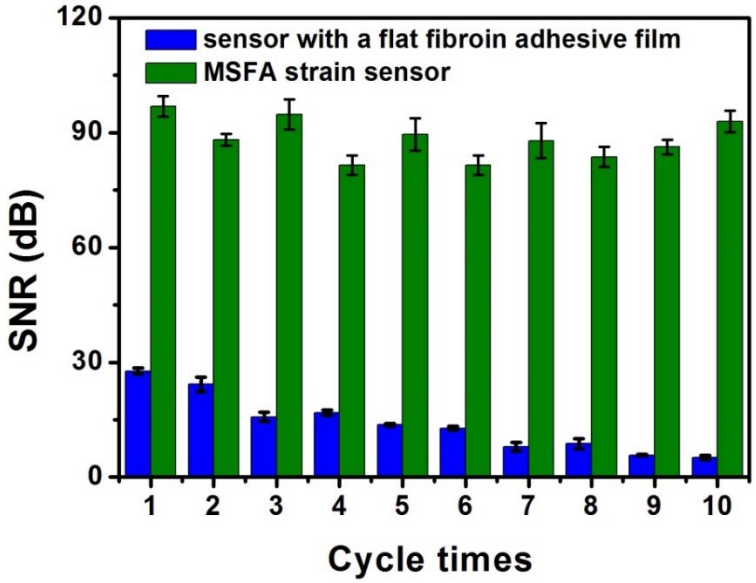

Figure S11 The signal-to-noise ratio (SNR) of a flexible strain sensor with the MSFA layer and with a flat fibroin adhesive layer in ten times repeating tests.

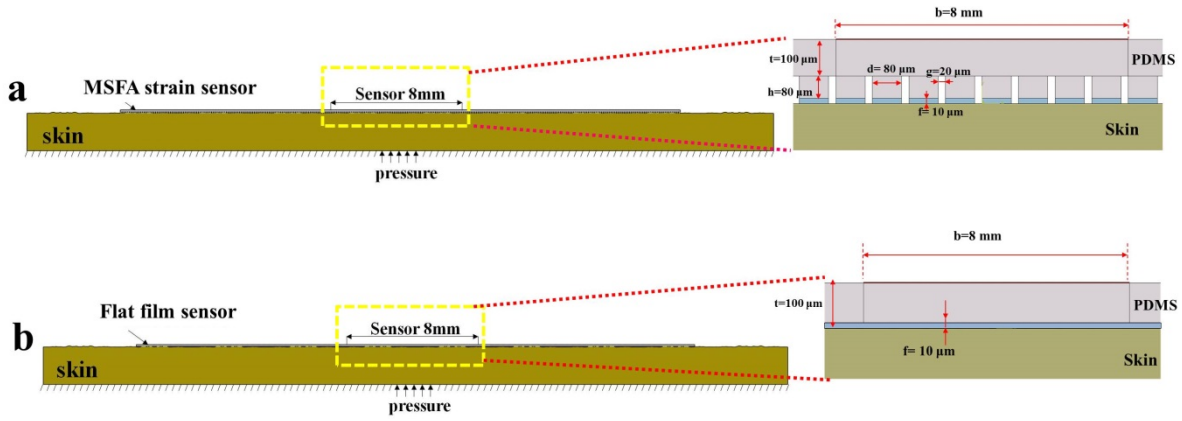

Figure S12 Schematics on the modeling detail and boundary conditions applied for (a) MSFA strain sensor and (b) the same strain sensor with a flat fibroin adhesive layer. A pressure is applied on the bottom center of the model to simulate the effect of pulse jump caused by blood pressure, while the other area of the bottom is fixed, to mimic the effect of muscle constrain on the skin.

References

(1) Kelly, R.; Hayward, C.; Avolio, A.; O'Rourke, M. Noninvasive Determination of Age-Related Changes in the Human Arterial Pulse. *Circulation* **1989,** *80*, 1652-1659.

(2) Choong, C. L.; Shim, M. B.; Lee, B. S.; Jeon, S.; Ko, D. S.; Kang, T. H.; Bae, J.; Lee, S. H.; Byun, K. E.; Im, J.; Jeong, Y. J.; Park, C. E.; Park, J. J.; Chung, U. I. Highly Stretchable Resistive Pressure Sensors Using a Conductive Elastomeric Composite on a Micropyramid Array. *Adv. Mater.* **2014,** *26*, 3451-3458.

(3) Pang, C.; Koo, J. H.; Nguyen, A.; Caves, J. M.; Kim, M. G.; Chortos, A.; Kim, K.; Wang, P. J.; Tok, J. B.; Bao, Z. Highly Skin-Conformal Microhairy Sensor for Pulse Signal Amplification. *Adv. Mater.* **2015,** *27*, 634-640.